

Synthesis of Calix[6]arene based XAD-4 Material for the Removal of Reactive Blue 19 from Aqueous Environments

Ashfaque Ali Bhatti,¹ Muhammad Afzal Kamboh,² Imam Bakhsh Solangi,¹ Shahabuddin Memon¹

¹National Center of Excellence in Analytical Chemistry, University of Sindh, Jamshoro 76080, Pakistan

²Department of Chemistry, Kohat University of Science and Technology, Kohat, Khyber Pakhtunkhwa, Pakistan

Correspondence to: S. Memon (E-mail: shahabuddinmemon@yahoo.com)

ABSTRACT: This study describes the synthesis of calix[6]arene (C6) appended Amberlite XAD-4 resin and its application for the removal of anthraquinone-based reactive blue 19 (RB-19) dye from aqueous environments. The C6-resin 5 was characterized with various analytical techniques, including Fourier transform infrared spectroscopy, scanning electron microscopy, thermogravimetric analysis, and elemental analysis. Adsorption experiments were carried out to investigate the effects of the pH, adsorbent dosage, electrolyte, contact time, and temperature on the adsorption of RB-19 dye onto the C6-resin 5. From the results, we observed that the percentage adsorption of the RB-19 dye was highly dependent on the concentration of electrolyte and the pH of the solution. The maximum adsorption was achieved at pH 9. The thermal study demonstrated that the adsorption process was endothermic and spontaneous in nature. The isothermic study showed that the adsorption behavior could be better demonstrated by the Langmuir and Dubinin and Radushkevich isotherm model. From field studies, it has been concluded that C6-resin 5 is an effective adsorbent for the removal of RB-19 dye. © 2013 Wiley Periodicals, Inc. *J. Appl. Polym. Sci.* 130: 776–785, 2013

KEYWORDS: adsorption; applications; dyes/pigments

Received 26 November 2012; accepted 18 February 2013; published online 4 April 2013

DOI: 10.1002/app.39214

INTRODUCTION

During the past few decades, with the swift proliferation of industry, the world's economy has improved remarkably and has touched a new skyscraping horizon.¹ However, an increase in industrial units is also responsible for high risks of environmental pollution.² The textile processing and dyestuff manufacturing industries particularly are considered a major source of environmental pollution in terms of water contamination.³ Until now, approximately more than 100,000 kinds of different dyes have been commercially prepared, and millions of tons of these dyestuffs are used annually.^{4,5} Among them, reactive dyes are a well-known and important class of dyestuffs. Because of some of the properties of reactive dyes, including their multiplicity of color shades, high degree of fastness, ease of application, brilliant colors, and nominal energy consumption, they are known as a robust class of synthetic colorants and are extensively used in the textile industry.⁶ Because of their ionic nature and water solubility, they are usually used for dyeing cellulose fibers, cotton, rayon, silk, wool, and also leather.⁷ A literature survey revealed that these dyes have a 75–80% fixing capacity and approximately 15–20% of the dyes are released during the dyeing process.^{8,9}

As we know, during the dyeing process, a huge quantity of water is used for dyeing, fixing, and washing purposes. According to recent reports, only the textile processing and dyestuff manufacturing industries discharge more than 2.80 million tons of textile dyes yearly in the form of industrial effluent.^{10,11} The waste effluent of dyeing and textile industries is usually a complex mixture of a variety of chemicals ranging from unreacted dyes to auxiliary chemicals.¹² The mixture of released colored effluent with fresh water not only causes human health threats but also poses a serious threat to the natural environment. This contamination brings about considerable nonaesthetic pollution, and the presence of these dyes in trace quantities, that is, below 1 mg/L, is clearly visible and is considered as toxic to human and aquatic life.^{13,14} The presence of these colored bodies causes some chemical reactions, such as oxidation and hydrolysis, in the wastewater phase that may cause eutrophication, which can reduce the light penetration and create derogatory effects on photosynthesis.¹⁵ By virtue of their aromatic nature, most of the dye molecules are resistant to biological and chemical degradation.¹⁶ Moreover, the fused aromatic structures of anthraquinone-based reactive dyes makes them a highly persistent group of colorants, which can persist for a long time in wastewater.¹⁷

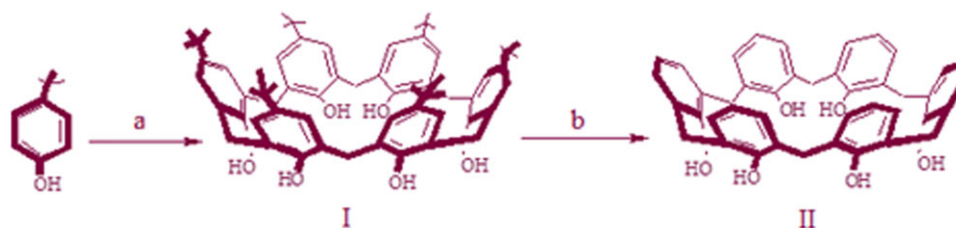


Figure 1. Synthesis of C6 (II): (a) HCHO/OH⁻ and (b) AlCl₃-phenol/toluene. [Color figure can be viewed in the online issue, which is available at wileyonlinelibrary.com.]

The toxicity of colored contaminated effluent has been extensively reviewed.^{18–20}

Hence, the treatment of such wastewaters has become a matter of great concern, and it is vital to develop sound and cost-effective treatment technologies to flush these undesired materials out of the effluent to provide a clean and safe environment. A variety of techniques, including membrane filtration, coagulation/flocculation, ion exchange, advanced oxidation, flotation, chemical reduction, biosorption, and biodegradation, have been employed to remediate dyes from wastewater.^{21,22} In comparison with other methods, its simplicity, fastness, cost effectiveness, and reusability makes the adsorption process the most valuable and authentic method.¹⁷ A lot of research has been undertaken to develop a variety of cheaper and more effective adsorbent materials. These include natural and synthetic polymers, such as polysaccharides, chitin, chitosan, starch and its derivatives, activated carbon, peat, silica (SiO₂), and fly ash, but their use is limited in terms of adsorption efficiency and reusability.^{23–25}

From this point of view, those in supramolecular chemistry have searched for a solution and pursued molecular frameworks that can play a fundamental role in the production of sophisticated molecules containing various functionalities and possessing different binding sites for dyestuffs. This was achieved with the innovative development of the macrocyclic molecules named *calixarenes*.²⁶ Consequently, the chemical immobilization of calix[*n*]arene moieties onto the XAD-4 surface increases its reusability and provides it with enormous applications in the separation sciences. XAD-4 based resins are chemically, physically, and thermally stable under different experimental environments and have received much attention for the architecture of new and efficient chelating resins.^{27–29} Thus, in this study, we synthesized a calix[6]arene (C6) based XAD-4 resin and investigated its adsorption efficiency for reactive blue 19 (RB-19) dye. Various parameters, including the effects of the dosage, contact time, pH, and temperature on the adsorption capacity of the C6-resin 5, were monitored.

EXPERIMENTAL

Chemicals

RB-19 dye and wastewater samples used as adsorbates in this study were obtained from a commercially available source and industrial effluents, respectively. Hence, the pH of the solution was adjusted by the mixture of an appropriate amount of HCl or NaOH (0.1N) into the solutions. Analytical thin-layer chromatography was performed on precoated silica gel plates (Merck

PF254, Darmstadt, Germany). Sodium hydroxide, formaldehyde, diphenyl ether, acetone, acetic acid, toluene, and ethanol were purchased from Merck. Toluene was freshly distilled before use. Amberlite XAD-4 resin was purchased from Fluka (Bush, Switzerland). All aqueous solutions were prepared with deionized water that had been passed through a Milli-Q system (Elga Model Classic UVF, United Kingdom).

Equipment

The melting points were determined on a Gallenkamp melting-point apparatus (model MFB 595. 010M, England). Elemental analyses were performed with a CHNS elemental analyzer (model Flash EA 1112, Rndano, Milan, Italy). IR spectra were recorded on a Thermo-Nicolet 5700 Fourier transform infrared (FTIR) spectrometer (Fitchburg, WI) with KBr pellets. Ultraviolet–visible (UV–vis) spectra were obtained with a PerkinElmer Lambda 35 UV–vis spectrophotometer (Shelton, CT). Scanning electron microscopy (SEM) studies were performed with a JSM-6490 instrument. The pH measurements were made with a pH meter (781 pH/ion meter, ΩMetrohm Metrohm, Herisau Switzerland) with a glass electrode and an internal reference electrode. A Gallenkamp thermostated automatic mechanical shaker (model BKS 305-101) was used for the batch study.

Synthesis

p-*tert*-Butylcalix[6]arene (I) and C6 (II), as depicted in Figure 1, were synthesized according to previously reported procedures.^{30,31}

Immobilization of C6 (II) onto Modified Amberlite XAD-4 Resin (4). A diazonium derivative of Amberlite XAD-4 (4), as shown in Figure 2, was prepared according to our previously reported methods.^{32,33} The immobilization of C6 (II) onto the diazonium derivative of Amberlite XAD-4 (4) was carried out as follows.

The diazotized resin 4 (5 g) was reacted with C6 (II; 5 mmol, 2.12 g) in 400 mL of glacial acetic acid and acetone (3 : 1) at 0–3°C for 30 h. The resulting grayish colored beads of the C6-resin 5 were filtered off, washed with distilled water and chloroform to remove excess or unreacted C6 (II), and then dried in a vacuum oven. An amount of 7.02% of C6 (II) was immobilized onto the surface of Amberlite XAD-4. Finally, the immobilization was confirmed by fundamental analytical techniques, including FTIR, SEM, thermogravimetric analysis (TGA), and elemental analysis.

ANAL. Calcd for C₆₀H₅₇N₂O₄·2H₂O: C, 79.44%; H, 6.28%; N, 3.88%. Found: C, 79.51%; H, 6.55%; N, 3.72%.

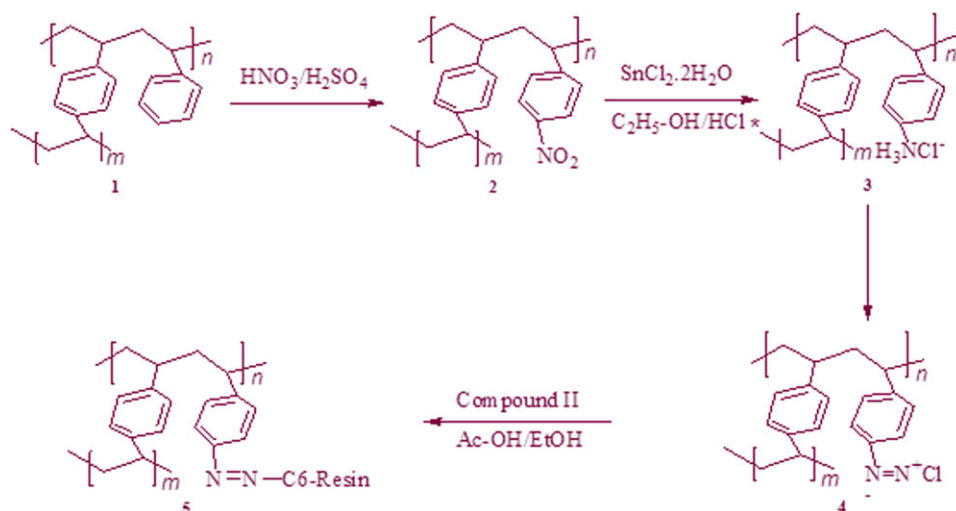


Figure 2. Immobilization of C6 (II) onto the modified Amberlite XAD-4 resin 5 (Ac-OH = acetic acid; EtOH = ethanol). [Color figure can be viewed in the online issue, which is available at wileyonlinelibrary.com.]

Adsorption Procedures

Batch Method. Batchwise adsorption experiments were carried out for the RB-19 dye at room temperature, that is, $25 \pm 1^\circ\text{C}$. A sample solution (10 mL) containing 10 mL of RB-19 dye (2×10^{-5} M) was placed in a 25-mL Erlenmeyer glass stoppered flask. C6-resin 5 (75 mg) was added, and the mixture was equilibrated for a fixed period of time (60 min) at a constant speed of 160 rpm in a horizontal shaker. Finally, the resin was filtered off, and the adsorbed RB-19 dye was analyzed by UV-vis spectrophotometry at its particular wavelength, that is, 592 nm. The percentage adsorption of RB-19 dye was calculated as follows:

$$\text{Adsorption}(\%) = \frac{C_i - C_f}{C_i} \times 100 \quad (1)$$

where C_i is the initial concentration of the solution before the adsorption (mol/L) and C_f is the final concentration after the adsorption of the RB-19 dye (mol/L).

RESULTS AND DISCUSSION

Characterization

FTIR Spectra. Because the structures of the newly synthesized C6-based diazotized XAD-4 (C6-resin 5) and previously reported calix[4]arene-based diazotized XAD-4 resin were similar, the FTIR spectra was analyzed by a comparison with a previously reported calix[4]arene-based diazotized XAD-4 resin.³³ Figure 3 shows the FTIR spectrum of the newly synthesized C6-resin 5. The band observed at 3451 cm^{-1} was assigned to —OH stretching. The bands observed at 2928, 1705, 1606, 1505, 1444, and 1368 cm^{-1} were assigned to the asymmetrical stretching of the C—H, N=N, C=C, C—C, and —C—N groups, respectively. For C6-based diazotized XAD-4 resin 5, the characteristic vibration peaks for the band at 1706 cm^{-1} for N=N, while last two bands for —C—N groups were clearly observed (Figure 4) at 1706, 1448, and $1368/\text{cm}$, respectively. These diagnostic peaks confirmed the immobilization of C6 (II) onto resin 4.

SEM. The morphological characteristics of the C6-resin 5 was evaluated with SEM (Figure 4) by the application of a 5-kV electron acceleration voltage. Figure 4 represents the SEM micrographs of the C6-resin 5 at high magnification. From these images, it is clear that the surface of the beads was covered with a layer of immobilized species. Thus, the deposition of foreign material, that is, C6 (II), onto the surface of the XAD-4 beads confirmed the immobilization.

TGA. TGA was used to examine the thermal stability of the C6-based XAD-4 resin 5, as presented in Figure 5. The thermal degradation curve of the C6-resin 5 showed two main steps. The first step, ranging from 35 to 130°C , was allocated to the loss of physically adsorbed water, and the second step, ranging from 200 to 450°C , was recognized as C6 (II) ring combustion.

Adsorption Study of the RB-19 Dye

Effect of the adsorbent dosage. The adsorbent dosage is a very crucial parameter; it helps in the evaluation of the adsorption capacity of an adsorbent for a fixed given initial concentration of the adsorbate at operating conditions. The effect of the adsorbent dosage (pure Amberlite XAD-4 and resin) for the

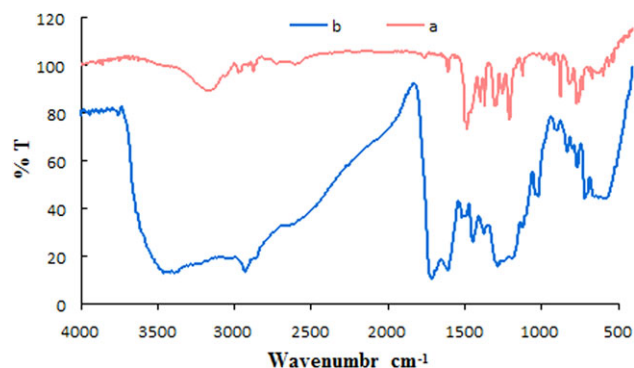


Figure 3. FTIR spectra of the (a) C6 (II) and (b) C6-resin 5. [Color figure can be viewed in the online issue, which is available at wileyonlinelibrary.com.]

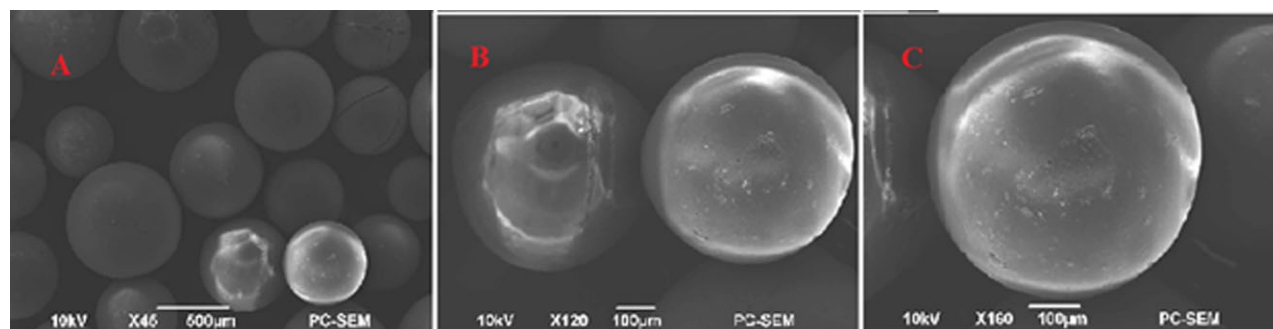


Figure 4. Different SEM images of the surface of the immobilized C6-resin 5 at (a) 500, (b) 100, and (c) 100 μm . [Color figure can be viewed in the online issue, which is available at wileyonlinelibrary.com.]

removal of the RB-19 dye was investigated through the variation of the dosage from 25 to 150 mg with a fixed concentration ($2 \times 10^{-5} \text{M}$) of adsorbate, that is, RB-19 dye. Figure 6 shows the percentage adsorption of RB-19 dye, which increased with increasing adsorbent dosage; more than 70% adsorption was observed with 75 mg of adsorbent (i.e., C6-resin 5).

pH effects of the adsorption of the RB-19 dye. Because adsorption phenomena involve the interaction between the surface of the adsorbent and adsorbate, during the dye adsorption, the pH is considered a driving parameter because the solution pH affects both the aqueous chemistry and the surface binding sites of the adsorbent.³⁴ Therefore, the pH effect from 3 to 11 for the removal of the RB-19 dye was investigated (Figure 7). From the results, we deduced that basic media was more favorable for the adsorption of RB-19 dye onto the C6-resin 5. The newly synthesized resin showed a maximum adsorption at pH 9, whereas above pH 9, dramatic changes occurred, and the adsorption of the RB-19 dye decreased remarkably. This was due to the complex structural nature of the anthraquinone RB-19 dye, which contained a variety of functional groups. The RB-19 dye bore a sulfonate group, and in a basic environment as a

result of the dissociation of sulfonate groups, the RB-19 dye became negatively charged and interacted with sodium ions as Figure 16 describes it. In the same way, the adsorbent contained phenolic hydroxyl groups of the C6 moiety in the C6-resin 5; at basic pH, the phenolic hydroxyl groups were deprotonated; this made the C6-resin 5 anionic in nature. In this scenario, a favorable environment was provided to the negatively charged resin for electrostatic interactions with metal ions of the adsorbate; this facilitated adsorption. Moreover, the phenoxide ions in the C6 framework had the capability to bind sodium ions, and this implied an anion-pair extraction mechanism in which Na^+ coordinated with the phenoxide ions along with the dye anions, and the rest of the dye molecule inserted itself into the hydrophobic calixarene cavity. In contrast, at higher pH, the lower adsorption was attributed to the increase in the concentration of OH^- ions, which competed with the negative outer sites of the adsorbent.^{35,36}

Influence of the NaCl concentration on the adsorption of dye. Ionic strength is an electrostatic parameter that largely affects the dye removal efficiency; therefore, electrostatic interactions were monitored by the incorporation of electrolytic

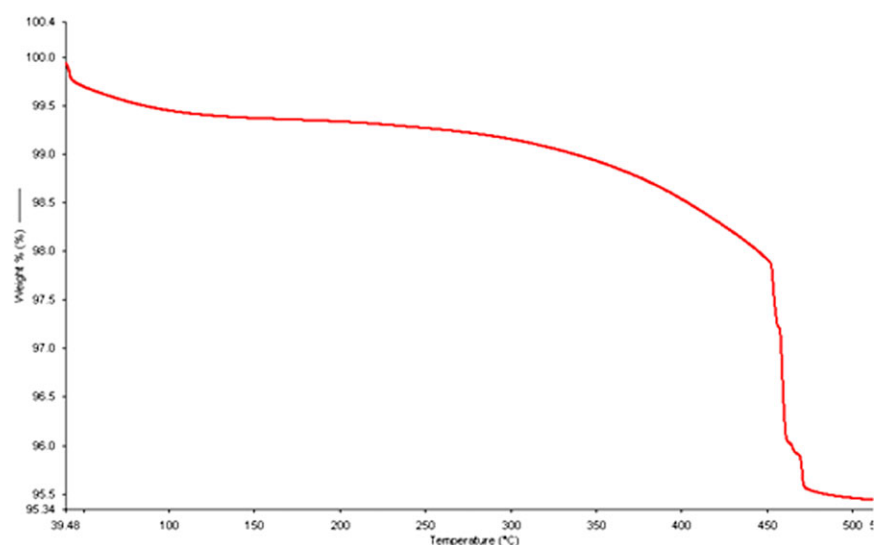


Figure 5. TGA curve C6-resin 5 at a constant temperature under an N_2 atmosphere. [Color figure can be viewed in the online issue, which is available at wileyonlinelibrary.com.]

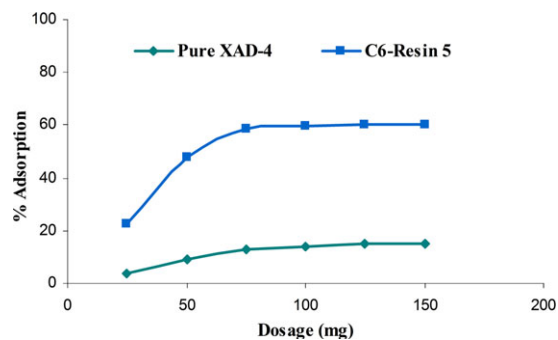


Figure 6. Effect of the adsorbent dosage (25–150 mg) on the percentage adsorption of the RB-19 dye (contact time of 60 min, 0.3M NaCl, and 10 mL of dye at a concentration of $2 \times 10^{-5}M$). [Color figure can be viewed in the online issue, which is available at wileyonlinelibrary.com.]

concentrations ranging from 0 to 0.5 mol/L, as shown in Figure 8. It is clear from these results that the adsorption capacity of the C6-resin 5 increased rapidly from 0 to 0.3 mol/L, and an almost maximum adsorption was achieved at 0.3 mol/L. However, there was only a minor increase in the percentage of adsorption that took place from 0.3 to 0.5 mol/L. Consequently, the increase in the percentage adsorption with respect to the increase in the electrolytic concentration could be explained as follows: NaCl provided an ionic balance between the two phases and increased the solubility of the dye molecule through a common ion effect; this resulted in an increased and facilitated transport to the organic phase.³⁷

Adsorption isotherm. The adsorption isotherm is an important factor describing the actual surface chemistry, and it is a measure of the extent of the surface being adsorbed by the adsorbent material at given conditions.³⁸ Furthermore, isotherm models describe the adsorption capacity, structure of the adsorbed layer, and interaction between the adsorbate and adsorbent.³⁹ Thus, the experimental data were incorporated into isotherm models, namely, the Langmuir, Freundlich, and Dubinin and Radushkevich (D–R) models, with optimized parameters to assess the adsorption capacity of the C6-resin 5 for the RB-19 dye. The linearized forms of the equations of the isotherms are as follows^{40–42}

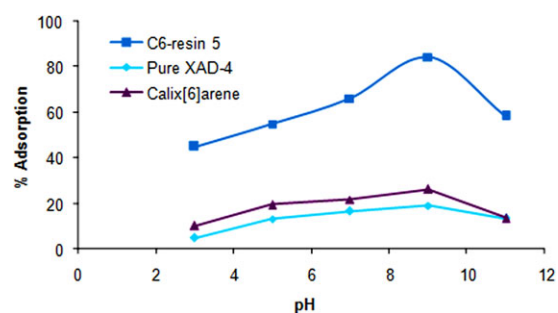


Figure 7. pH effect on the adsorption of RB-19 (75 mg of adsorbent, contact time of 60 min, 0.3M of NaCl, and 10 mL of dye at a concentration of $2 \times 10^{-5}M$). [Color figure can be viewed in the online issue, which is available at wileyonlinelibrary.com.]

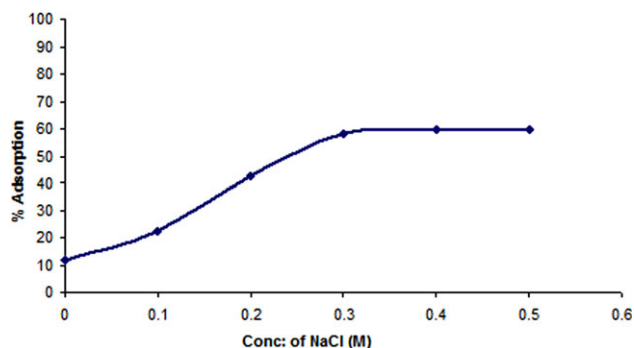


Figure 8. Effect of the NaCl concentration on the adsorption of RB-19 (75 mg of adsorbent, contact time of 60 min, and 10 mL of dye at a concentration of $2 \times 10^{-5}M$). [Color figure can be viewed in the online issue, which is available at wileyonlinelibrary.com.]

$$\left(\frac{C_e}{C_{ads}}\right) = \left(\frac{1}{Qb}\right) + \left(\frac{C_e}{Q}\right) \quad (2)$$

$$\ln C_{ads} = \ln A + \frac{1}{n} \ln C_e \quad (3)$$

$$\ln C_{ads} = \ln X_m - \beta \varepsilon^2 \quad (4)$$

where β constant related to energy, ε polanyi potential, C_{ads} is the amount of adsorbate at the adsorbent surface (mol/g); C_e is the amount of adsorbate in the liquid phase at equilibrium (mol/L). The maximum sorption capacity (Q), b relates to enthalpy of the sorption, A is a sorption capacity constant and $1/n$ is another constant related with energy or intensity of sorption, and the monolayer adsorption capacity (X_m) are Langmuir, Freundlich, and D–R constants, respectively, which could be calculated experimentally.

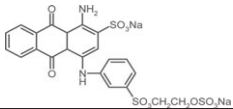
The Langmuir isotherm predicts the structurally homogeneous surface of the adsorbent where all of the adsorptive sites are identical and energetically equivalent. The theoretical X_m could be determined from parameters of the linearized form of the model [eq. (2)] and was used by the plot of C_e/C_{ads} versus C_e , which exhibited a straight line. From the value of the regression coefficient, we observed that the adsorption data followed the Langmuir isotherm equation. The essential characteristics of the Langmuir isotherm can be expressed by the dimensionless constant called the *equilibrium parameter* (R_L), as illustrated in the following equation:

$$R_L = \frac{1}{(1 + bC_i)} \quad (5)$$

where b is the Langmuir constant and C_i is the initial concentration of RB-19 (mol/L). The R_L value indicates favorability and was calculated as 0.05–0.23 (Table 1); this implied that high adsorption took place favorably onto the surface of the C6-resin 5 (Figure 9).

Similarly, the Freundlich isotherm was applied to elucidate the heterogeneity of the surface; this implied a multilayer adsorption.⁴¹ This model is distinguished by its heterogeneity factor (i.e., $1/n$). So, we calculated the values of the constants of the Freundlich adsorption model by plotting the graph of $\ln C_{ads}$ (mol/g) versus \ln

Table I. Main Characteristics of RB-19

| | |
|--------------------|---|
| Chemical structure |  |
| CI generic name | CI RB-19 |
| Alternate name | Remazol Brilliant Blue R |
| Molecular formula | C ₂₂ H ₁₆ O ₁₁ N ₂ S ₃ Na ₂ |
| Molecular weight | 626.5 g/mol |
| λ _{max} | 592 nm |

Wavelength at which maximum absorption occur.

C_e (mol/L). From the intercept and slope, the values A and 1/n were evaluated and are compiled in Table I (Figure 10).

The D–R isotherm is generally used to differentiate between physical and chemical adsorption mechanisms.⁴² Compared to the Langmuir isotherm model, it imagines heterogeneity over the surface. In the analysis of the D–R isotherm model factor (C), the polynic potential can be evaluated as follows:

$$\epsilon = RT \ln \left(1 + \frac{1}{C_e} \right) \quad (6)$$

where T is the absolute temperature (K), R is the gas constant (kJ mol/K), and E is the mean adsorption energy and can be written as

$$E = \frac{1}{\sqrt{-2\beta}} \quad (7)$$

When C_e² was plotted against ln C_{ads} (mol/g), a linear graph with a correlation coefficient (R²) of 0.99 (Table I) was obtained (Figure 11). X_m was found to be 0.99, and E was justified as 12.9 kJ/mol; this suggested that the adsorption of RB-19 onto the C6-resin 5 was purely chemical in nature.

Table II shows the experimental constant values calculated from the Langmuir, Freundlich, and D–R isotherm equations. The regression coefficient (R²) values obtained from these equations applied to the adsorption of RB-19 dye onto C6-resin 5 and indicated that the Langmuir and D–R models yielded much better applicability than the Freundlich isotherm model. Furthermore, the data implied the applicability of the Langmuir and D–R isotherms and explained the surface monolayer coverage of the RB-19 dye on the surface of the C6-resin 5.

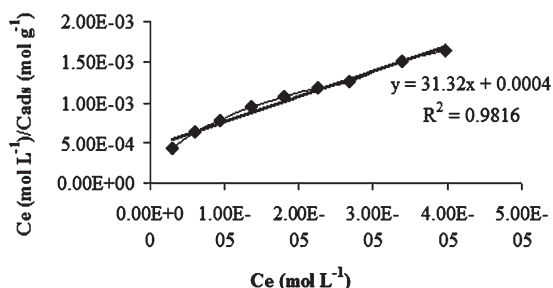


Figure 9. Langmuir adsorption isotherm of the RB-19 dye onto C6-resin 5.

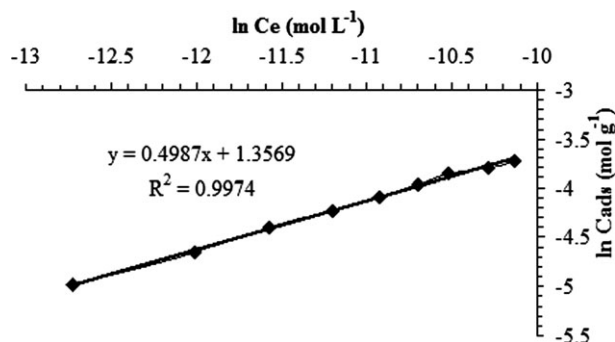


Figure 10. Freundlich adsorption isotherm of the RB-19 dye onto C6-resin 5.

Adsorption kinetics. In kinetic studies, the rate of adsorption of RB-19 onto the C6-resin 5 was determined with four kinetic models, the pseudo-first-order, pseudo-second-order, intraparticle diffusion (Reichenberg equation), and Moris–Waber models. The plots of the adsorbed amount of the RB-19 dye onto the C6-resin 5 at time t (q_t) versus t at temperatures of 303–313 K were made to evaluate the adsorption kinetics of RB-19 onto the C6-resin 5. Moreover, the adsorption mechanism was evaluated by application of the pseudo-first-order and pseudo-second-order type kinetic models (Table III).^{43,44}

It was estimated that at 303–313 K, the adsorption rate of RB-19 onto the C6-resin 5 likely followed pseudo-second-order rate equations [eqs. (8) and (9)]:

$$\ln (q_e - q_t) = \ln q_e - kt \quad (8)$$

A linear relationship was observed for the pseudo-first-order with the plots of log(q_e - q) against t, where q_t and q_e are adsorbed amounts of the RB-19 dye (mg/g) onto the C6-resin 5 at t and at equilibrium, respectively. K₁ (/min) is the pseudo-first-order rate constant. From the slopes and intercepts of the linear plots, the values of K₁ (/min) and q_e (mg/g) were obtained. Initially, the dye was adsorbed rapidly, and then equilibrium was attained within 15 min. K₁ is the adsorption rate constant. Thus, the K₁ values were obtained from linear plots. The adsorption rate constants were determined from slopes of the plots. The K₁ values are listed in Table II for the RB-19 adsorption onto the C6-resin 5 and determined at 303–313 K.

In the solid phase, the adsorption capacity based on the pseudo-second-order equation is expressed as follows:

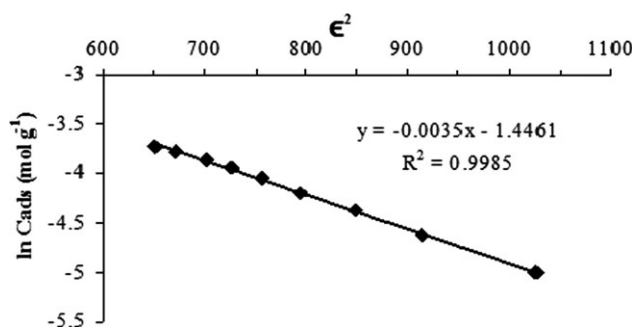


Figure 11. D–R adsorption isotherm of the RB-19 dye onto C6-resin 5.

Table II. Langmuir, Freundlich, and D-R Characteristic Constants for the RB-19 Dye

| Langmuir | | | | Freundlich | | | D-R | | |
|------------|-----------------------|------------------------|----------------|------------|------|----------------|------------------------|------------|----------------|
| Q (mmol/g) | b (mol/L) | R _L (mol/L) | R ² | A (mol/g) | 1/n | R ² | X _m (mol/g) | E (kJ/mol) | R ² |
| 31.15 | 1.6 × 10 ⁵ | 0.05-0.23 | 0.99 | 3.9 | 0.49 | 0.98 | 0.99 | 12.9 | 0.99 |

$$dq/dt = K_2(q_e - qt)^2 \quad (9)$$

where K_2 is the rate constant of the second-order sorption. For the same boundary conditions, the integrated form of eq. (9) becomes eq. (10):

$$\frac{t}{q_t} = \left(\frac{t}{K_2 q_e^2} \right) + \left(\frac{1}{q_e} \right) \quad (10)$$

Second-order kinetics could be applied by the plotting of t/q_t against t of eq. (10); this yielded a straight line, and q_e and K_2 were determined from the slope and intercept of the plot. In Table II, the kinetic parameters and the correlation coefficients of the kinetic models are shown. These were clear, although there was quite a sufficient value of correlation coefficient ($R^2 = 0.86$) for the first-order kinetic model at various temperatures, that is, 303, 308, and 313 K, but the q_e value was not reasonable, so the adsorption of RB-19 onto the C6-resin 5 did not fit in this equation. Although in the case of the pseudo-second-order model, the experimental data fit significantly well and provided better correlation coefficients than the pseudo-first-order model for the C6 resin 5. The pseudo-first-order model is based on the assumption that the rate-limiting step may be physical adsorption involving hydrogen bonding between adsorbate and adsorbent.

The Reichenberg equation⁴⁵ was checked for RB-19 dye adsorbed via either film interaction or intraparticle diffusion mechanism. The equation is as follows:

$$Q = 1 - 6e - B_t/\pi^2 \quad (11)$$

where $Q = q_t/q_e$, $B_t = \pi^2 D_i t^2/r^2$, q_t is the adsorbed concentration at t , q_e is the maximum adsorption capacity, and D_i is the effective diffusion coefficient of the adsorbate species onto the adsorbent at a particle value of B_p , which is the mathematical function of Q and can be evaluated for each value of Q with the following equation:

$$B_t = -0.4977 - \ln(1 - Q) \quad (12)$$

Table III. Comparison of the Pseudo-First-Order and Pseudo-Second-Order Kinetic Models

| Pseudo-first-order kinetic model | | | Pseudo-second-order kinetic model | | |
|----------------------------------|----------------|----------------|-----------------------------------|-------------------------|----------------|
| K ₁ | q _e | R ² | K ₂ | q _e | R ² |
| (1/min) | (mol/g) | | (1/min) | (g/mol min) | |
| 0.1497 | 2.43 | 0.86 | 1.93 × 10 ⁻¹⁵ | 1.75 × 10 ⁻⁵ | 0.99 |

Thus, the plot of B_t versus time t (Figure 12) follows the linearity from 0 to 15 min. For adsorption, a straight line of this plot was used to differentiate between the external transport (film diffusion) and intraparticle-transport-controlled rates.⁴⁶ The results clearly indicate that at different temperatures, all of the lines were linear and did not pass through the origin. This suggested that film diffusion was the rate-limiting process for RB-19 adsorption onto the C6-resin 5.

The kinetic adsorption was also examined with the Morris-Weber equation:⁴⁶

$$q_t = R_d \sqrt{t} \quad (13)$$

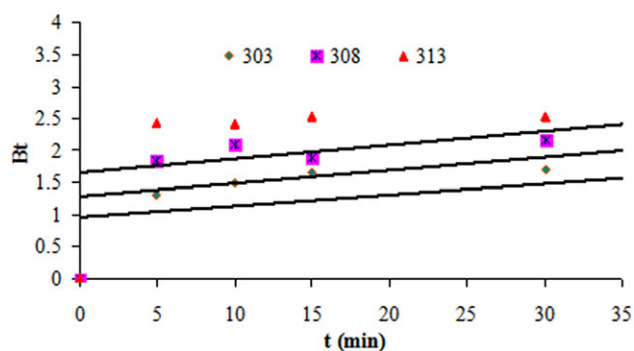
where q_t is the concentration of RB-19 adsorbed at t and R_d is the rate constant of intraparticle transport. q_t (mol/g) was plotted against \sqrt{t} , as shown in Figure 13.

From the slope of the plot in the initial stage (Figure 8), the values of R_d and the rate constants of intraparticle transport were estimated as 1.103, 1.364, and 1.165 mol g/ $\sqrt{\text{min}}$ with correlation coefficients of 0.938, 0.960, and 0.953, respectively, at 303–313 K.

Thermodynamics of adsorption. The thermodynamic parameters, including the change in enthalpy (ΔH), entropy (ΔS), and Gibbs free energy (ΔG), are the actual indicators for the practical application of a process, which can explain the mechanism of adsorption.⁴⁷ Thus, the effect of the temperature on the adsorption of the RB-19 dye onto the C6-resin 5 was studied at different temperatures (i.e., 303, 308, and 313 ± 1 K) under optimum conditions.

The thermodynamic parameters (ΔH , ΔS , and ΔG) were calculated from the slope and intercept of the linear plot of $\ln(q_d/C_e)$ versus $1/T$ under optimum conditions with the following equations:

$$\ln K_c = \frac{-\Delta H}{RT} + \frac{\Delta S}{R} \quad (14)$$

**Figure 12.** Reichenberg plot of the adsorption of the RB-19 dye at a temperature of 303–313 K onto C6-resin 5. [Color figure can be viewed in the online issue, which is available at wileyonlinelibrary.com.]

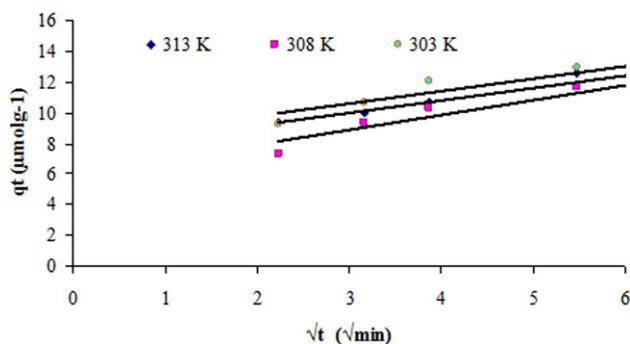


Figure 13. Morris–Weber plot for the adsorption of the RB-19 dye at a temperature of 303–313 K onto C6-resin 5. [Color figure can be viewed in the online issue, which is available at wileyonlinelibrary.com.]

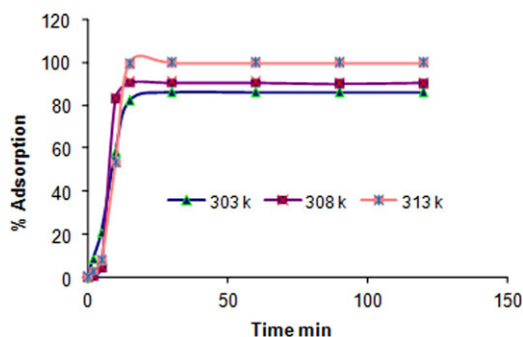


Figure 14. Adsorption curves of the RB-19 dye onto C6-resin 5 as a function of the shaking time at different temperatures from 303 to 313 K. [Color figure can be viewed in the online issue, which is available at wileyonlinelibrary.com.]

$$\Delta G = -RT \ln K_c \quad (15)$$

where K_c is equilibrium constant. From Figure 14, we concluded that the percentage adsorption increased with increasing temperature. The numerical values of ΔH and ΔS were calculated from a plot of $\ln K_c$ versus $1/T$ from eq. (14). From the ΔH and ΔS values, ΔG was determined from eq. (14). The values obtained from eqs. (14) and (15) are listed in Table IV. The ΔG value was negative as expected for a spontaneous process under applied conditions and confirmed that the RB-19 dye adsorbed spontaneously onto the surface of the C6-resin 5.

Moreover, endothermic nature of adsorption could be analyzed from the positive value of ΔH . In addition, the increase in the value of $\ln K_c$ (1.72, 2.34, and 2.96 at 303, 308, and 313 K,

Table IV. Thermodynamic Parameters for the Adsorption of the RB-19 Dye onto the C6-Resin 5

| ΔH (kJ/mol) | ΔS (kJ/mol/K) | ΔG (kJ/mol) | | |
|------------------------|--------------------------|---------------------|------------------|------------------|
| | | 303 K | 308 K | 313 K |
| 0.098 | 0.339 | -7.72 | -5.99 | -4.33 |
| | | $\ln K_c = 1.72$ | $\ln K_c = 2.34$ | $\ln K_c = 2.97$ |

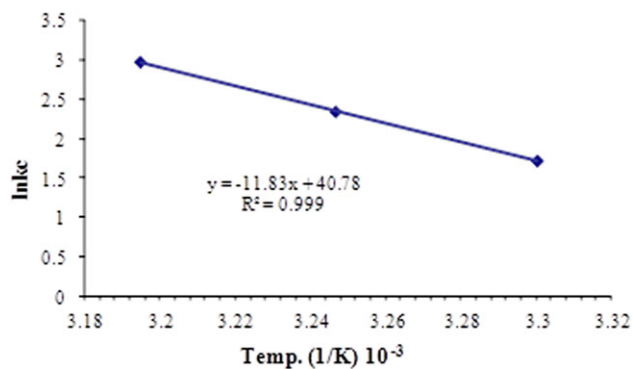


Figure 15. Effect of the temperature on the adsorption of the RB-19 dye onto C6-resin 5. [Color figure can be viewed in the online issue, which is available at wileyonlinelibrary.com.]

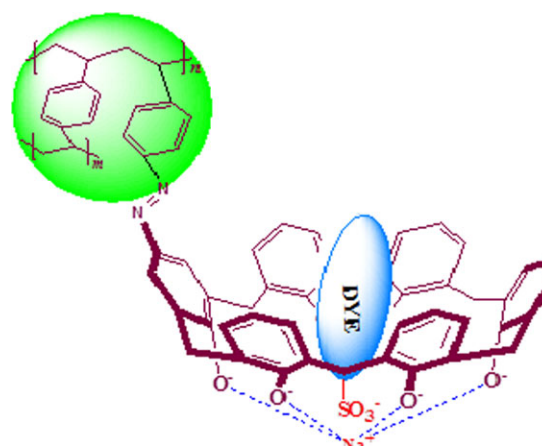


Figure 16. Proposed mechanism of the RB-19 dye adsorption. [Color figure can be viewed in the online issue, which is available at wileyonlinelibrary.com.]

respectively) with increasing temperature showed that the adsorption of the RB-19 dye onto the C6-resin 5 was an endothermic process. This suggested that the driving force for the adsorption process was a ΔS effect, and the slightly positive value of ΔS implied that there was an increase in randomness at the solid/solution interface during the adsorption of the RB-19 dye onto the C6-resin 5 (Figures 15 and 16).⁴⁷

Field Application of the C6-Resin 5

To ensure the C6-resin 5 as an efficient adsorbent for the removal of RB-19 dye from aqueous environments, a field study of C6-resin 5 for real wastewater samples containing RB-19 dye

Table V. RB-19 Dye Concentration in the Wastewater Samples before and after Treatment with the C6-Resin 5

| Sample | Concentration before treatment | Concentration after treatment | Removal (%) |
|--------|--------------------------------|-------------------------------|-------------|
| | 1 | 1.22×10^{-4} | |
| 2 | 8.61×10^{-5} | 3.02×10^{-5} | 64.92 |

Table VI. Comparison of the pH, TDS, Conductivity, and Salinity of the Wastewater Samples with C6-Resin 5

| Sample | Before treatment | | | | After treatment | | | |
|--------|------------------|------------|-----------------------------------|----------|-----------------|------------|-----------------------------------|----------|
| | pH | TDS (mg/L) | Conductivity ($\mu\text{S/cm}$) | Salinity | pH | TDS (mg/L) | Conductivity ($\mu\text{S/cm}$) | Salinity |
| 1 | 9.2 | 217 | 463 | 2.1 | 8.4 | 30 | 70.2 | 0 |
| 2 | 9.5 | 661 | 1400 | 0.5 | 8.8 | 110 | 231 | 0 |

Table VII. Adsorption Capacities of the Different Adsorbents Used for the Removal of the RB-19 Dye

| Adsorbent | T ($^{\circ}\text{C}$) | q_m | Langmuir constant (k_L) | References |
|--------------------------------------|----------------------------|----------------------------|-----------------------------|----------------------------------|
| Bentonite with a cationic surfactant | 20 | 3.30×10^{-4} mg/g | 2.89×10^{-4} L/mg | Adnan Özcan et al. ⁴⁸ |
| Agricultural waste | 25 | 12.39 mg/g | 0.278 L/mg | Mahmood et al. ⁴⁹ |
| Wheat bran | 20 | 97.1 mg/g | 0.162 L/mg | Çiçek et al. ⁵⁰ |
| <i>Candida rugosa</i> | 25 | 8 mg/g | mg/g | Polman et al. ⁵¹ |
| <i>Funalia trogii</i> | | 10.7 mg/g | | Chulhwan et al. ⁵² |
| <i>Pichia carsonii</i> | 20 | 5 mg/g | 2.03 L/mg | Polman et al. ⁵¹ |
| Canola hull | 30 | 2.0161 mmol/g | 0.2743 L/mg | Mahmoodi et al. ⁵² |
| Orange peel | | 25.0 mg/g | 0.075 | Ahmed et al. ⁵³ |
| Fly ash | | 17 mg/g | | Karaa et al. ⁵⁴ |
| Cuttlefish bone powder | 20 | 10.86 mg/g | 0.014 L/mg | Ghaneian et al. ⁵⁵ |
| Banana and orange peels | 30 | 20.6 mg/g | 32.6 L/mg | Annadurai et al. ⁵⁶ |
| C6-resin 5 | 25 | 31.15 mmol/g | 0.05–0.23 L/mg | This study |

was also carried out. Batch experiments were performed with 75 mg of C6-resin 5 and 10 mL of a real sample of effluent contaminated with RB-19 dye that was stirred at 160 rpm for 60 min at 30°C. The concentration of RB-19 dye was investigated before and after the treatment of dye waste effluent with the C6-resin 5 through UV–vis spectrophotometry at its particular wavelength, that is, 592 nm. The results are summarized in Table V.

From Table V, the lower concentration of RB-19 dye in the waste effluents after the treatment indicated that the C6-resin 5 was an efficient adsorbent and could successfully employed for the decontamination of RB-19 dye from aqueous environments (Table VI).

Comparison of Adsorbents

A comparative evaluation of the adsorbent capacity of the C6-resin 5 with various types of adsorbents for the adsorption of RB-19 is given in Table VII. The maximum adsorption capacity (q_m) of C6-resin 5 for RB-19 at pH 9.0 and 25°C was evaluated as 31.15 mmol/g. The data show that the adsorption capacity of the C6-resin 5 was relatively high compared with other reported adsorbent materials.^{48–56}

CONCLUSIONS

This study highlights the main features of the synthesis of C6-resin 5 and its application for the adsorption of RB-19 dye from aqueous media. Basic and advanced instrumental techniques, including FTIR spectroscopy, SEM, TGA, and elemental analysis, confirmed the synthesis of the C6-resin 5. The adsorp-

tion of RB-19 dye was highly pH dependent. Thermal studies clarified that the adsorption process was endothermic and spontaneous in nature. The adsorption of RB-19 dye tended to follow Langmuir and D–R isotherm models rather than the Freundlich isotherm. Moreover, the field studies also supported the C6-resin 5 as an effective adsorbent for the removal of RB-19 dye. Additionally, it also reduced other water quality parameters, including pH, total dissolved salts (TDS), conductivity, and salinity, near to those of drinking water. Hence, the results of this study signify that C6-resin 5 has a high capacity to adsorb RB-19 dye from contaminated wastewater.

ACKNOWLEDGMENTS

The authors thank the National Center of Excellence in Analytical Chemistry, University of Sindh, Jamshoro, Pakistan, for financial support of this work.

REFERENCES

- Gupta, V. K.; Suhas. *J. Environ. Manage.* **2009**, *90*, 2342.
- Olukanni, O. D.; Osuntoki, A. A.; Gbenle, G. O. *Afric. J. Biotech.* **2006**, *5*, 1984.
- Kalyani, D. C.; Telke, A. A.; Dhanve, R. S.; Jadhav, J. P. *J. Hazard. Mater.* **2009**, *163*, 742.
- Kamari, A.; Ngah, W. S. W.; Liew, L. *J. Environ. Sci.* **2009**, *21*, 302.
- Deveci, T.; Unyayar, A.; Mazmanci, M. A. *J. Mol. Catal. B* **2004**, *30*, 32.

6. Aspland, J. R. *Textile Dyeing and Coloration*; American Association of Textile Chemists and Colorists: Research Triangle Park, NC, **1997**; p 113.
7. Ahmed, H. A. *J. Text. Dye Print.* **1995**, 28, 24.
8. Lee, Y. H.; Pavlostathis, S. G. *Water Res.* **2004**, 38, 1852.
9. Lewis, D. M. *Rev. Prog. Color.* **1999**, 29, 28.
10. Ozmen, E. Y.; Erdmir, S.; Yilmaz, M.; Bahadir, M. *Clean* **2007**, 35, 619.
11. Kamboh, M. A.; Solangi, I. B.; Sherazi, S. T. H.; Memon, S. *J. Iran. Chem. Soc.* **2011**, 8, 279.
12. Rajkumar, D.; Song, B. J.; Kim, J. G. *Dyes Pigments* **2007**, 72, 7.
13. Couto, S. R. *Biotechnol. Adv.* **2009**, 27, 235.
14. Banat, I. M.; Nigam, P.; Singh, D.; Marchant, R. *Biores. Technol.* **1996**, 58, 227.
15. Asamudo, N. U.; Daba, A. S.; Ezeronye, O. U. *Afric. J. Biotechnol.* **2005**, 4, 1553.
16. Vandevivere, P. C.; Bianchi, R.; Verstraete, W. *J. Chem. Technol. Biotechnol.* **1998**, 72, 302.
17. Qiao, S.; Hu, Q.; Haghseresht, F.; Hu, X.; Lu, G. Q. *Sep. Purif. Technol.* **2009**, 67, 255.
18. Gnanamani, A.; Bhaskar, M.; Ganeshjeevan, R.; Chandrasekar, R.; Sekaran, G.; Sadulla, S.; Ganga, R. *Process. Biochem.* **2005**, 40, 3504.
19. Sponza, D. T. *J. Hazard. Mater.* **2006**, 138, 447.
20. Manning, B. W.; Cerniglia, C. E.; Federle, T. W. *Appl. Environ. Microbiol.* **1985**, 50, 15.
21. Latif, L.; Noor, S.; Sharief, M. Q.; Najeebullah, M. *J. Chem. Soc. Pak.* **2010**, 32, 124.
22. Ghaedi, M.; Hossainian, H.; Montazerohori, M.; Shokrollahi, A.; Shojaipour, F.; Soylak, M.; Purkait, M. K. *Desalination* **2011**, 281, 233.
23. Ghaedi, M.; Shokrollahi, A.; Tavallali, H.; Shojaiepoor, F.; Keshavarzi, B.; Hossainian, H.; Soylak, M.; Purkait, M. K. *Toxicol. Environ. Chem.* **2011**, 93, 449.
24. Kamboh, M. A.; Yilmaz, M. *Desalination* **2013**, 310, 67.
25. Chatterjee, D.; Patnam, V. R.; Sikdar, A.; Moulik, S. K. *J. Chem. Eng. Data.* **2010**, 55, 5657.
26. Yilmaz, M.; Memon, S.; Tabakci, M.; Bartsch, R. A. In *New Frontiers in Polymer Research*; Bregg, R. K, Ed.; Nova: New York, **2006**; p 172.
27. Jain, V. K.; Sait, S. S.; Shrivastav, P.; Agrawal, Y. K. *Talanta* **1997**, 45, 404.
28. Solangi, I. B.; Memon, S.; Bhangar, M. I. *J. Hazard. Mater.* **2010**, 176, 192.
29. Soylak, M.; Elci, L.; Dogan, M. *J. Trace Microprobe Tech.* **2001**, 19, 344.
30. Gutsche, C. D.; Iqbal, M.; Stewart, D. *J. Org. Chem.* **1986**, 51, 745.
31. Gutsche, C. D.; Lin, L. G. *Tetrahedron* **1986**, 42, 1640.
32. Solangi, I. B.; Memon, S.; Bhangar, M. I. *Anal. Chim. Acta.* **2009**, 638, 153.
33. Kamboh, M. A.; Solangi, I. B.; Sherazi, S. T. H.; Memon, S. *J. Hazard. Mater.* **2009**, 172, 239.
34. Errais, E.; Duplay, J.; Darragi, F.; Rabet, I.; Aubert, A.; Huber, F.; Morvan, G. *Desalination* **2011**, 275, 81.
35. Xue, Y.; Hou, H.; Zhu, S. *J. Chem. Eng.* **2009**, 147, 279.
36. Kamboh, M. A.; Solangi, I. B.; Sherazi, S. T. H.; Memon, S. *Desalination* **2011**, 268, 89.
37. Crini, G. *Biores. Technol.* **2003**, 90, 198.
38. McCash, E. M. *Surface Chemistry*; Oxford University Press: New York, **2001**; p 177.
39. Dąbrowski, A. *Adv. Colloid Interface Sci.* **2001**, 93, 224.
40. Langmuir, I. *J. Am. Chem. Soc.* **1918**, 40, 1403.
41. Freundlich, H. *Colloid and Capillary Chemistry*; Methuen: London, **1926**; p 414.
42. Polanyi, M. *Trans. Faraday Soc.* **1932**, 28, 316.
43. Haribabu, E.; Upadhya, Y. D.; Upadhyay, S. N. *Int. J. Environ. Stud.* **1993**, 43, 176.
44. Ho, Y. S.; McKay, G. *Process. Biochem.* **1999**, 34, 456.
45. Reichenberg, J. D. *J. Am. Chem. Soc.* **1953**, 75, 597.
46. Morris, W. J.; Weber, C. *J. Saint Eng. Div. Am. Soc. Civ. Eng.* **1963**, 89, 59.
47. Memon, G. Z.; Bhangar, M. I.; Akhtar, M. *J. Colloid Interface Sci.* **2007**, 315, 40.
48. Özcan, A.; Ömeroğlu, Ç.; Erdoğan, Y.; Özcan, A. S. *J. Hazard Mater.* **2007**, 140, 179.
49. Abassi, M.; Asl, N. R. *J. Iran. Chem. Res.* **2009**, 2, 230.
50. Çiçek, F.; Özer, D.; Özer, A.; Özer, A. *J. Hazard Mater.* **2007**, 146, 416.
51. Polman, J. K.; Breckenridge, C. R. *Text. Chem. Color* **1996**, 28, 31.
52. (a) Chulhwan, P.; Lee, M.; Lee, B.; Kim, S. W.; Howard, A. C.; Lee, J.; Kim, S. *Biochem. Eng. J.* **2007**, 36, 59; (b) Mahmoodi, N. M.; Arami, M.; Bahrami, H.; Khorramfar, S. *J. Appl. Polym. Sci.* **2011**, 120, 3003.
53. Ahmed, S. A. S.; Khalil, L. B.; El-Nabarawy, T. *Carb. Lett.* **2012**, 13, 220.
54. Karaa, S.; Aydinera, C.; Demirbasb, E.; Kobayaa, M.; Dizgea, N. *Desalination* **2007**, 212, 293.
55. Ghaneian, M. T.; Momtaz, M.; Dehviri, M. *J. Health Res.* **2012**, 1, 11.
56. Annadurai, G.; Juang, R. S.; Lee, D. J. *J. Hazard Mater.* **2002**, 92, 274.